applied sciences

MDPI

Article

High-Temperature Superconductivity in the Lanthanide Hydrides at Extreme Pressures

Yao Wei, Francesco Macheda, Zelong Zhao, Terence Tse, Evgeny Plekhanov *, Nicola Bonini * and Cedric Weber *

Theory and Simulation of Condensed Matter (TSCM), King's College London, The Strand, London WC2R 2LS, UK; yao.wei@kcl.ac.uk (Y.W.); francesco.macheda@kcl.ac.uk (F.M.); zelong.zhao@kcl.ac.uk (Z.Z.); wai_hei_terence.tse@kcl.ac.uk (T.T.)

* Correspondence: evgeny.plekhanov@kcl.ac.uk (E.P.); nicola.bonini@kcl.ac.uk (N.B.); cedric.weber@kcl.ac.uk (C.W.)

Abstract: Hydrogen-rich superhydrides are promising high-T_c superconductors, with superconductivity experimentally observed near room temperature, as shown in recently discovered lanthanide superhydrides at very high pressures, e.g., LaH_{10} at 170 GPa and CeH_9 at 150 GPa. Superconductivity is believed to be closely related to the high vibrational modes of the bound hydrogen ions. Here, we studied the limit of extreme pressures (above 200 GPa) where lanthanide hydrides with large hydrogen content have been reported. We focused on LaH_{16} and CeH_{16}, two prototype candidates for achieving a large electronic contribution from hydrogen in the electron–phonon coupling. In this work, we propose a first-principles calculation platform with the inclusion of many-body corrections to evaluate the detailed physical properties of the Ce–H and La–H systems and to understand the structure, stability, and superconductivity of these systems at ultra-high pressure. We provide a practical approach to further investigate conventional superconductivity in hydrogen-rich superhydrides. We report that density functional theory provides accurate structure and phonon frequencies, but many-body corrections lead to an increase of the critical temperature, which is associated with the spectral weight transfer of the f-states.

Keywords: superconductivity; electronic interactions; high pressure

Citation: Wei, Y.; Macheda, F.; Zhao, Z.; Tse, T.; Plekhanov, E.; Bonini, N.; Weber, C. High-Temperature Superconductivity in the Lanthanide Hydrides at Extreme Pressures. *Appl. Sci.* **2022**, *12*, 874. https://doi.org/10.3390/app12020874

Academic Editor: Leonid Burakovsky

Received: 13 December 2021
Accepted: 13 January 2022
Published: 15 January 2022

1. Introduction

In the research of condensed matter [1], pressure is a fundamental thermodynamic variable that determines the state of matter and plays an important role in the field. The discovery of new materials and therefore applications for industrial use makes up an important part of modern innovation. As a basic thermodynamic parameter, pressure demonstrates the ability to activate semi-core electrons, empty orbitals, and non-atom-centred quantum orbitals on interstitial sites, changing a given element's chemistry, thus resulting in a plethora of novel and previously unexpected occurrences, for example the generation of new types of functional materials that deviate from those under atmospheric pressure (101.325 kPa) [2].

Currently, hydrogen-rich materials have garnered much attention in regard to obtaining superconductivity at high temperatures and have led to much theoretical and experimental work on the search for the high-temperature superconductivity of hydrides under high pressure [3]. The chemical pre-compression method, proposed by Neil Ashcroft in 2004, has led to the key realisation that hydrogen-rich compounds are a new potential class of high-temperature superconductors [4]. As investigating the high-temperature superconductivity of metallic hydrogen is highly challenging [5], most scholars have instead redirected focus to the synthesis and properties of hydride-rich compounds instead. Recently, the realisation of very-high-temperature superconductivity, near room temperature, was discovered in hydrogen disulphide [6,7] and lanthanum hydrogen [8–10], an important set of milestones.

Hydrogen disulphide was previously believed to undergo dissociation under high pressures and was not heavily considered as a potential superconductor. However, recent theoretical work has suggested that dissociation would not occur, but that on the contrary, the material would become superconducting [11]. Inspired by this discovery, Drozdov et al. compressed sulphur hydride in a diamond anvil cell and showed that hydrogen sulphide would indeed form a superconductor when compressed with a T_c of up to 200 K [12].

Armed with this new knowledge, researchers have expanded their search to include lanthanide hydrides under pressure, with notable examples such as La–H [13] and Y–H [14]. The Fermi density and thus superconductivity in La–H systems are determined not only by the *d* orbital La electrons and the *s* orbital H electrons, but also by the *f* orbital electrons of lanthanum [15].

Using DFT, studies have found that the face-centred cubic (FCC) form of LaH_{10} is a good metal, with various bands crossing the Fermi level that form a high electronic density at the Fermi level [16]. In contrast, for the YH_{10} system, only the *d* orbital Y electrons and the *s* orbital H electrons become major contributors to the Fermi density at high pressures [17]. As external pressure destabilises the localised La-4*f* more than the other orbitals (La-6*s*, La-5*d*), the latter populates when pressure is applied, leading to possible novel emergent quantum states associated with the strong electronic correlations. In particular, it was purported that the La–H system has a unique high T_c with *f* electrons at the Fermi level [18].

The effects of electronic localisation and hybridisation apply for all high-density compounds, and this is the hallmark of a wide family of similar materials signified by transition metals, lanthanides, and rare-earth elements. Many-body effects give rise to a number of unique and interesting phenomena in similar systems, such as high-temperature superconductivity in cuprates and the metal–insulator transition in vanadates at ambient temperature [19]. The Zaanen–Sawatzky–Allen theory offers a categorisation of transition metal periodic solids in terms of their correlation' strengths and has provided a good knowledge base, though deep understanding of the hydride's characteristics distant from ambient conditions remains hitherto difficult and incomplete [20].

Therefore, in order to identify new hydrogen-rich high-T_c superconductors at the lowest possible pressure, the use of quantitative theoretical computations is required. Superconductivity in these potential compounds is mediated by the interaction between the highly intense lattice vibrations of hydrogen atoms and the localised electrons. An accurate description of this interaction necessitates fine descriptions of the electronic characteristics, which are infamous for being difficult for such correlated *f* systems, treating both itinerant and localised electrons on the same footing.

Several theoretical aspects, including the electron–phonon coupling strength λ, phonon dispersion relations, electron spectral weight, and cross-terms between electron–electron and electron–phonon interactions are corrected with electronic correlations.

Here, we propose a pragmatic first-principles-calculation-consistent platform that uses many-body corrections for the electronic spectral weight, which then feeds into adjusted estimates of T_c. The many-body corrections to phonon dispersion are typically less drastic than the corrections to the electronic spectra, as correlation effects can shift the f spectral weight over several eV. Furthermore, since their full treatment is beyond reach, the scope of this work was restricted to only correcting the electronic spectra.

In this manuscript, we show that the many-body corrections in *f* orbital systems could cause significant changes, with spectral weight shifts in the order of one electron volt. We evaluated the precise physical properties of the La–H and Ce–H systems, giving special care to the effect of correlations on the spectral properties. We found that LaH_{16} and CeH_{16} have stable P6/mmm space group crystal structures at pressures up to 250 GPa. Additionally, for the recently discovered cerium hydride, we predicted a comparatively high T_c, evaluated using our pre-established hierarchical approach [21].

2. Discussion

The idea that hydrogen-rich compounds could be potential high-T_c superconductors dates back to the turn of the millennium, when chemical pre-compression was proposed as a viable way to reduce the metallisation pressure of hydrogen in the presence of other elements, leading to observed T_c exceeding 150 K in the LaH_{16} system. This indicates compressed hydrogen-rich compounds as potential room-temperature superconductors.

The genesis of superconductivity in these hydrides is known to originate from electron–phonon interactions. The characteristic phonon frequency, the electron–phonon coupling strength, the density of states at the Fermi level, and the Coulomb pseudopotential μ^* are the four factors that define T_c according to BCS theory. Density functional theory, using conventional pseudo-potentials, such as the PBE, is widely acknowledged to provide an accurate explanation of lattice dynamics. However, for compounds with weakly hybridised and localised f electrons, such as La and Ce, where many-body corrections are required, DFT is known to have difficulties in dealing with strong electronic correlations.

We applied a density functional theory technique combined with dynamical mean-field theory (DMFT) in this study. The charge and spin local fluctuations, which are important for the local paramagnetic moment of lanthanide elements, are readily corrected by DMFT. DMFT is used to account for changes in the orbital character at the Fermi surface caused by spectral weight transfer related to Hubbard f band splitting. This influences low-energy electron–electron scattering processes via phonon momentum transfer, as stated in the Methods Section, according to the Allen–Dynes formalism.

P6/mmm-LaH_{16} and P6/mmm-CeH_{16} show very little dependence on pressure at 100 GPa. The phonon DOS of P6/mmm-LaH_{16} and P6/mmm-CeH_{16} computed at 250 GPa is shown in Figure 1, Panels (a) and (b), and the structural parameters are shown in Table A1. Then, we investigated the impact of various DMFT electronic charge self-consistency schemes (see Figure 1c,d). We found that correlation effects have a significant impact on $\alpha^2F(\omega)$. In particular, we compared: (i) PBE density functional theory; (ii) DFT+DMFT with the full-charge self-consistent formalism (DFT+DMFT+CSC). We used the Koster–Slater interaction vertex for La and Ce correlated manyfold, with typical values for $U = 6$ eV and $J = 0.6$ eV. Interestingly, the full-charge self-consistent DMFT provides a large increase of the superconducting temperature (see Panels (e) and (f) in Figure 1). This confirms that many-body effects have a sizeable contribution to the prediction of the superconducting temperatures in lanthanide hydrides. Note that we used $U = 6$ eV and $J = 0.6$ eV throughout the rest of the paper.

We focused on the LaH_{16} and CeH_{16} P6/mmm systems at 250 GPa. Although DMFT readily provides important corrections to the electronic structure, it is worth investigating how DMFT affects the structural qualities. Calculating forces with limited atomic displacement is not tractable due to the high computing overhead of performing many-body adjustments. Recently, we developed a method for the calculation of forces within DMFT, allowing for ultra-soft and norm-conserving pseudopotentials in the underlying DFT [22]. This opens up new possibilities for systems with heavy components that are not well-suited to all-electron computations. The structure relaxation at 250 GPa is seen in Figure 2. Typically, we obtained corrections for the bond lengths of the order of 5%.

The many-body effects tend to slightly shorten the La–H and Ce–H bonds, somehow increasing the La–H and Ce–H covalency. At the same time, this La–H and Ce–H bond length reduction is accompanied by a moderate increase in the H–H distance. This behaviour is opposite what we previously found in CeH_9, where both the Ce–H and H–H bonds were longer within the DMFT treatment [21].

The changes highlighted above stem directly from a spectral weight transfer induced by many-body corrections (see Figure 3a,b). In DFT, the La system is described by a two-band system in absence of a long-range magnetic order. We note that DFT is a single Slater determinant approach, and hence cannot capture the role of paramagnetism, with an associated magnetic multiplet (fluctuating magnetic moment). Such effects typically induce a splitting of spectral features into satellites, as observed in Figure 3c,d, with a resulting

large increase of the f character at the Fermi level. As sharp La features occur near the Fermi level, we emphasise that a higher level of theory is required to correctly capture the superconducting properties. For instance, in our calculations, the one-shot (DFT+DMFT) and full-charge self-consistent approach (DFT+DMFT+CSC) induces a small shift of the sharp La feature at the Fermi level, which in turn mitigates the f character increase at the Fermi level.

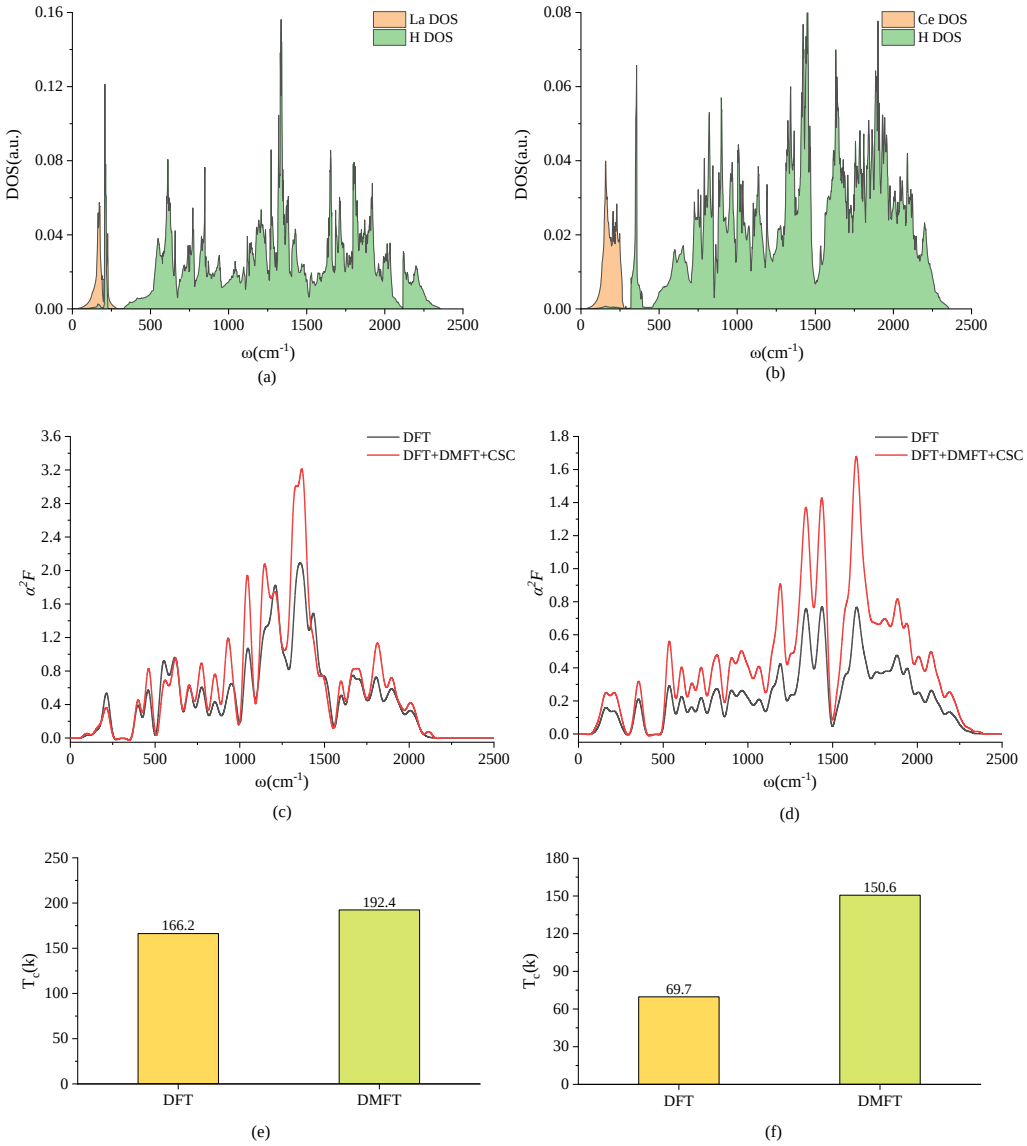

Figure 1. Many-body corrections to the superconducting temperature. We report (**a**) phonon density of states for LaH_{16}; (**b**) phonon density of states for CeH_{16}; (**c**,**d**) Eliashberg function $\alpha^2F(\omega)$ for LaH_{16} and CeH_{16}; the spectral weight at the Fermi level is obtained at different levels of approximation: (i) DFT PBE (black line) and (ii) with the full-charge self-consistent formalism (DFT+DMFT+CSC, red line); (**e**,**f**) The superconducting temperature T_c obtained by the Allen and Dynes formalism for LaH_{16} and CeH_{16} at 250 GPa. We obtain a theoretical estimate for LaH_{16} as $T_c = 166.2$ K by DFT and $T_c = 192.4$ K by DMFT, as well as a theoretical estimate for CeH_{16} as $T_c = 69.7$ K by DFT and $T_c = 150.6$ K by DMFT. The full-charge self-consistent DMFT provides a large increase of the superconducting temperature, and the physical value of the Hund's coupling for La and Ce is $U = 6$ eV and $J = 0.6$ eV. All calculations were performed in the P6/mmm phase of LaH_{16} and CeH_{16} at 250 GPa.

The role of f orbitals appears to be very important for the superconducting properties in rare-earth hydrates [21]. That is why in the present paper, in addition to LaH_{16} with the formally empty La f shell, we studied also cerium hydrate (CeH_{16}) with one f electron in the atomic Ce configuration. We checked that both systems remain stable at pressures up to at least 250 GPa.

We report in Figure 4 the DFT+DMFT+CSC framework applied to CeH_{16} in the P6/mmm phase at 250 GPa. We attributed the decrease in T_c to a higher f occupation, which shifts the chemical potential away from the f spectral features present near the Fermi level (see Figure 4c,d). Furthermore, Figure 4b shows that there is no obvious sudden change at the Fermi level, but there is an obvious mutation at the Fermi level in Figure 4d, which is around 7(1/eV); the correction of DMFT greatly affects the Tc of Ce.

Our findings point to a possible path for increasing T_c in lanthanide hydrides: an increase in the f character at the Fermi level in DFT+DMFT, which is associated with a lower degree of La–H and Ce–H covalency and a lower degree of hybridisation, which, in turn, is a marker for a higher superconducting temperature in these systems.

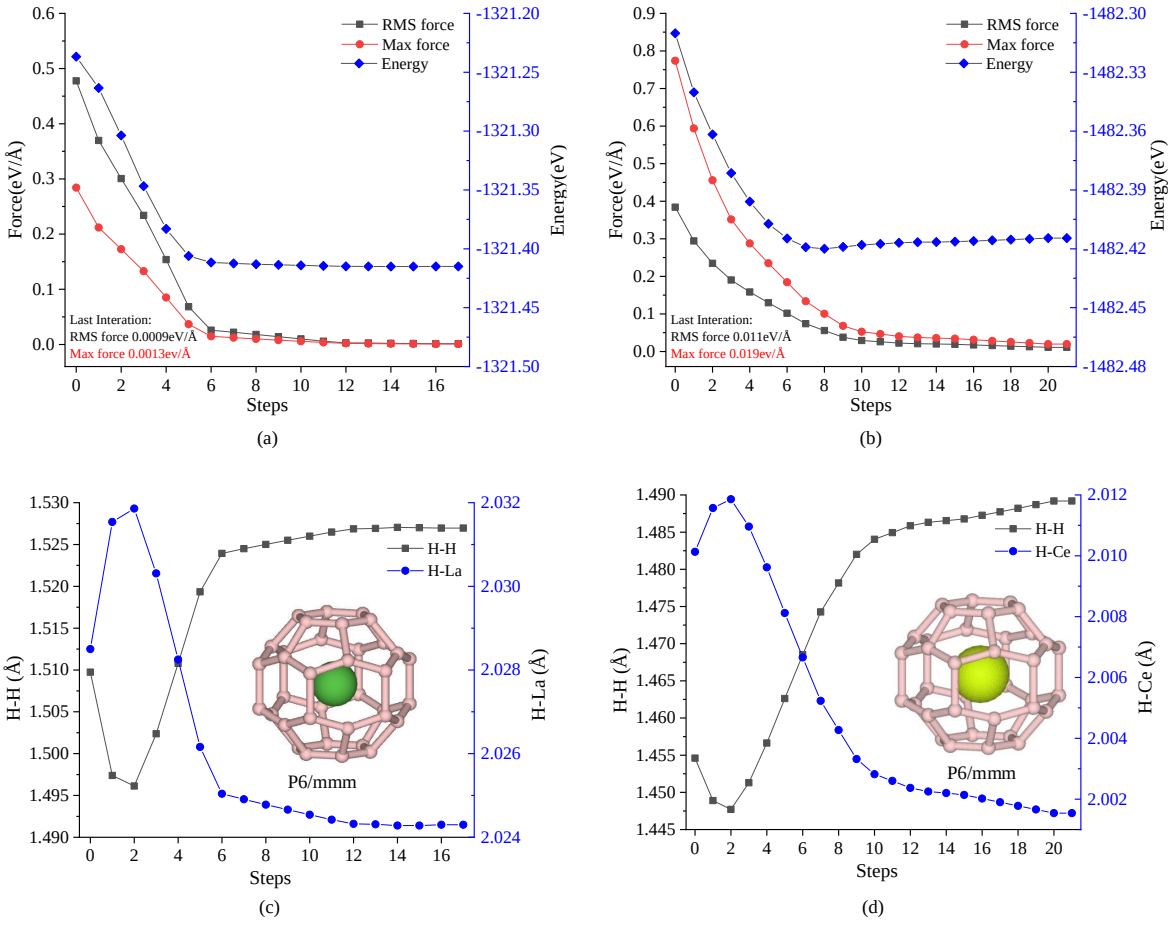

Figure 2. Structural relaxation of clathrate lanthanides with many-body corrections. We report the structural relaxation of the LaH_{16} (**a**,**c**) and prototype CeH_{16} (**b**,**d**) compounds. All calculations are performed at 250 GPa. The volume density is obtained by the equation of state in DFT+DMFT+CSC that provides very similar results to PBE (not shown). Internal coordinates are relaxed with DFT+DMFT+CSC, building upon the recent implementation of DFT forces for ultra-soft pseudo-potentials. We report the forces and total energies obtained during the structural optimisation, respectively, in (**a**,**b**) for LaH_{16} (CeH_{16}). Convergence is obtained within 25 iterations. The shortest H–H and Ce–H bond lengths increase throughout the structural optimisation (see **c**,**d** for La and Ce hydrides, respectively).

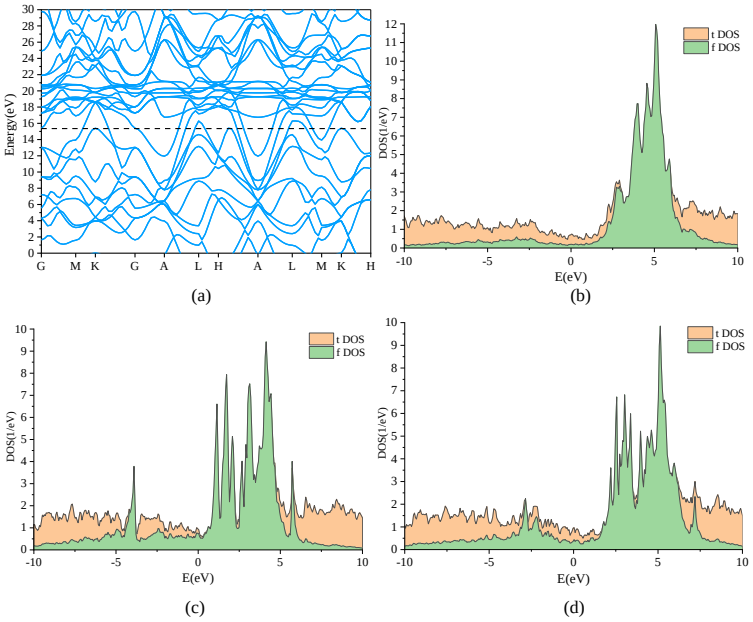

Figure 3. Spectral weight transfer induced by many-body corrections. (**a**) Electronic band structure and (**b**) density of states obtained by DFT calculations. $tDOS$ and $fDOS$ denote the spectral weight obtained by the imaginary part of respectively the lattice and f impurity Green function, corresponding to the spectral weight traced over all orbitals and traced over the f orbitals, respectively. In (**c**,**d**), we show the energy-resolved spectral weight, obtained respectively by the one-shot DFT+DMFT and the full-charge self-consistent DFT+DMFT+CSC. All calculations were performed in the P6/mmm phase of LaH_{16} at 250 GPa.

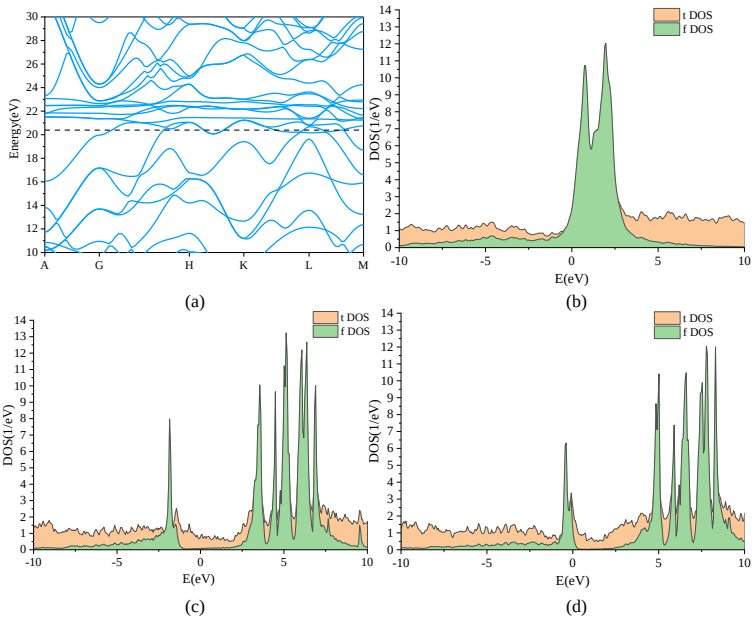

Figure 4. Spectral weight transfer induced by many-body corrections. (**a**) Electronic band structure and (**b**) density of states obtained by DFT calculations. $tDOS$ and $fDOS$ denote the spectral weight obtained by the imaginary part of respectively the lattice and f impurity Green function, corresponding to the spectral weight traced over all orbitals and traced over the f orbitals, respectively. In (**c**,**d**), we show the energy-resolved spectral weight, obtained respectively by the one-shot DFT+DMFT and the full-charge self-consistent DFT+DMFT+CSC. All calculations were performed in the P6/mmm phase of CeH_{16} at 250 GPa.

3. Methods

Figure 5 depicts our theoretical approach. We present a schematic overview of the theoretical platform's principal elements and their interrelationships. Our method establishes a modular framework for high-pressure material screening. Firstly, Crystal structure AnaLYsis by Particle Swarm Optimization (CALYPSO) provided the stoichiometric compositions via Gibbs enthalpies for the equation of state and convex hull [23]. Inter-operability between Quantum Espresso (QE) [24,25] was accomplished through input file format conversion, pseudopotentials, and **k**-point grids. The many-body corrections were provided by core libraries via the DMFT quantum embedding, which resulted in corrected forces [22] and total free energies [26,27].

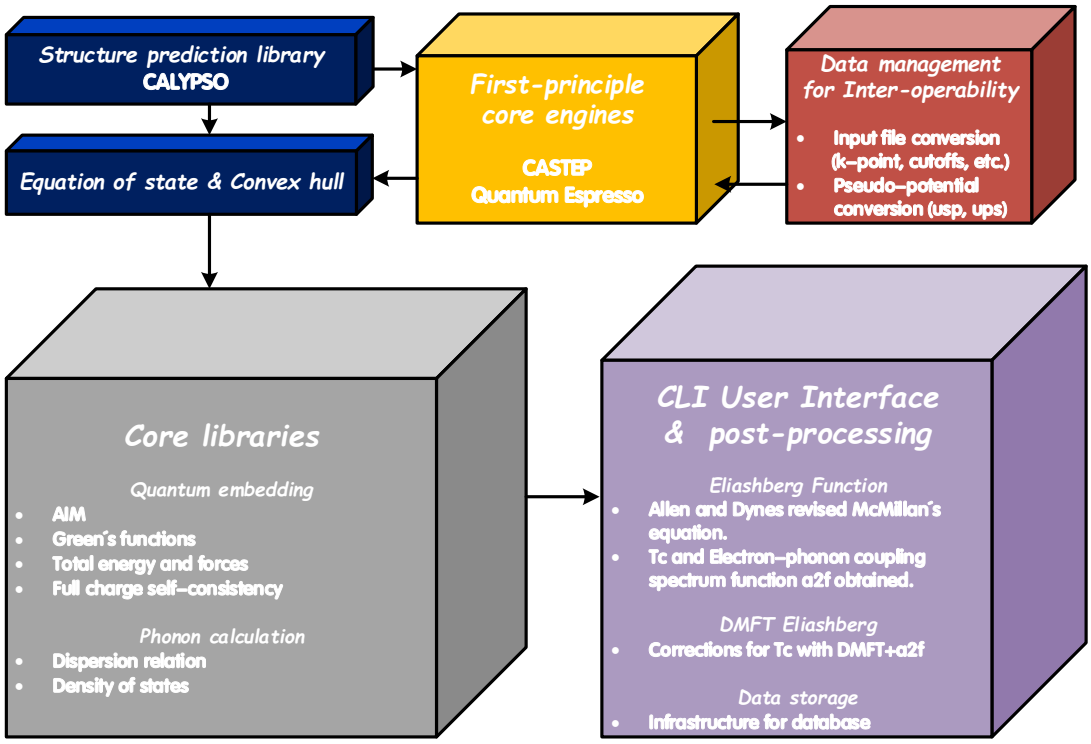

Figure 5. DFT inter-operability for a consistent many-body platform. Schematic overview of the main modules of the theoretical platform and its interrelations. Firstly, structures are predicted by Crystal structure AnaLYsis by Particle Swarm Optimization (CALYPSO), via Gibbs enthalpies for the equation of state and convex hull. The underlying core engines are the CASTEP and Quantum Espresso DFT software. Inter-operability between QE and CASTEP is achieved via format conversion of input files, pseudo-potentials, and **k**-point grids. Core libraries are used to provide the many-body corrections, via quantum embedding, which in turn provides corrected forces and energies. In post-processing, the Eliashberg function and superconducting T_c are obtained with the DMFT+a2F approach. Finally, data are archived for future usage in hdf5.

The underlying structure relaxations were carried out using the QE and CASTEP packages in the framework of DFT and using the Perdew–Burke–Ernzerhof generalised gradient approximation (PBE-GGA) [28,29]. Norm-conserving pseudopotentials were used to describe the core electrons and their effects on valence orbitals [30]. Valence electron configurations of $5s^2 5p^6 5d^1 6s^2$, $5s^2 5p^6 4f^1 5d^1 6s^2$ (i.e., with explicitly included f electrons), and $1s^1$ were used for the La, Ce, and H atoms, respectively. A plane-wave kinetic-energy cut-off of 1000 eV and dense Monkhorst–Pack **k**-point grids with a reciprocal space resolution of $12 \times 12 \times 12$ were employed in the calculation.

Phonon frequencies and superconducting critical temperature were calculated using density functional perturbation theory as implemented in QE [31]. The **k**-space integra-

tion (electrons) was approximated by a summation over a $20 \times 20 \times 12$ uniform grid in reciprocal space, with the Methfessel–Paxton smearing scheme, using a temperature of k_BT = 0.05 eV for self-consistent cycles and relaxations; the same grid ($20 \times 20 \times 12$) was used for evaluating DOS and coupling strength. Dynamical matrices and λ were calculated on a uniform $5 \times 5 \times 3$ grid in **q**-space for P6/mmm-LaH_{16} and P6/mmm-CeH_{16}.

In post-processing, the superconducting transition temperature T_c was estimated using the Allen–Dynes modified McMillan equation [32]:

$$T_c = \frac{\omega_{\log}}{1.2} \exp\left[\frac{-1.04(1+\lambda)}{\lambda - \mu^*(1+0.62\lambda)}\right] \tag{1}$$

where μ^* is the Coulomb pseudopotential. The electron–phonon coupling strength λ and $\omega_{\log}$ were calculated as:

$$\omega_{\log} = \exp\left[\frac{2}{\lambda}\int \frac{d\omega}{\omega}\alpha^2F(\omega)\log(\omega)\right], \tag{2}$$

$$\lambda = \sum_{\mathbf{q}\nu}\lambda_{\mathbf{q}\nu} = 2\int \frac{\alpha^2F(\omega)}{\omega}d\omega. \tag{3}$$

In the Allen–Dynes formalism, the Eliashberg function $\alpha^2F(\omega)$ is obtained by summing over all scattering processes at the Fermi level mediated by phonon momentum transfer and reads [33]:

$$\alpha^2F(\omega) = N(\epsilon_F)\frac{\sum_{\mathbf{k_1},\mathbf{k_2}}|M_{\mathbf{k_1},\mathbf{k_2}}|^2\delta(\omega-\omega_{\mathbf{q}\nu})\delta(\epsilon_{\mathbf{k_1}})\delta(\epsilon_{\mathbf{k_2}})}{\sum_{\mathbf{k_1},\mathbf{k_2}}\delta(\epsilon_{\mathbf{k_1}})\delta(\epsilon_{\mathbf{k_2}})}. \tag{4}$$

Here, $N(\epsilon_F)$ is the DOS at the Fermi level, $\omega_{\mathbf{q}\nu}$ is the phonon spectrum of a branch ν at momentum $\mathbf{q} = \mathbf{k_2} - \mathbf{k_1}$, $\epsilon_{\mathbf{k_1}}$ and $\epsilon_{\mathbf{k_2}}$ are electronic band energies referred to the Fermi level, while $M_{\mathbf{k_1},\mathbf{k_2}}$ are the electron–phonon coupling matrix elements. Many-body effects introduce a change of spectral character at the Fermi level, where electronic correlations induce a mass enhancement and introduce a finite lifetime, due to incoherence. In the spirit of the DMFT scissors, we corrected the DFT bands with the renormalised DMFT band picture:

$$\alpha^2F(\omega) = \mathcal{A}_{tot}\frac{\sum_{\mathbf{k_1},\mathbf{k_2}}|M_{\mathbf{k_1},\mathbf{k_2}}|^2\delta(\omega-\omega_{\mathbf{q}\nu})\mathcal{A}(\mathbf{k_1})\mathcal{A}(\mathbf{k_2})}{\sum_{\mathbf{k_1},\mathbf{k_2}}\mathcal{A}(\mathbf{k_1})\mathcal{A}(\mathbf{k_2})}, \tag{5}$$

where $\mathcal{A}_{tot}$ and $\mathcal{A}(\mathbf{k})$ are respectively the total and **k**-momentum resolved spectral weights at the Fermi level. This approach is denoted as *DMFT+a2F* in the workflow.

Within the DFT+DMFT quantum embedding approach, the DFT Kohn–Sham eigenstates were used in the calculation of the DMFT Green function [21,34]. We used atomic projectors to define the Anderson impurity model (AIM), which was successively solved within the Hubbard-I approximation. A breadth of quantum solvers is readily available in the TRIQS open-source platform [35,36]. In the full-charge self-consistent approach (DFT+DMFT+CSC), the Kohn–Sham potentials were calculated from the DMFT electronic density, obtained using the DMFT occupancies. Upon DMFT convergence, total energies and forces were calculated using the Green function and self-energy. All DFT calculations in this work were carried out using the pseudopotential formalism.

4. Conclusions

We created a methodology for estimating the superconducting temperature in lanthanide hydrides with many-body corrections and investigated a novel type of stable high-temperature superconducting material, CeH_{16}. The DMFT charge self-consistency, which involves many-body adjustments to the local charge density in first-principles calculations, was used to restore a consistent theoretical framework. A change in the spectral

weight of the f states caused a rise in the predicted superconducting temperature, which influenced the spectral character at the Fermi level. In this research, we obtained a theoretical estimate for LaH16 as T_c = 166.2 K by DFT and T_c = 192.4 K by DMFT, as well as a theoretical estimate for CeH16 as T_c = 69.7 K by DFT and T_c = 150.6 K by DMFT, and we also discussed the capabilities for relaxing lanthanide hydrides within the DMFT formalism, built on our recent developments providing DMFT forces for underlying ultra-soft and norm-conserving pseudopotentials, despite the fact that many-body corrections have so far been limited to the electronic contributions to the Eliashberg function. The latter gives structural insights, and we found that many-body effects on the lattice have negligible impacts at high pressures, since the DFT structures and pressures are similar to their DMFT counterparts. Although a comprehensive treatment of phonons at the DMFT level is out of reach for such complicated materials, the latter shows that many-body adjustments to the electronic component are responsible for the strong corrections of T_c. We investigated the aliovalent effect and discovered that compared to iso-structural La hydride and Ce hydride, an increase in the f character at the Fermi level leads to an increase in superconducting temperature, which is a compelling observation for future explorations of f systems as high-T_c superconductors. Our method is general and provides a modular framework for interoperating common first-principles software, such as the freely accessible CASTEP+DMFT and Quantum Espresso codes, with a tiny numerical footprint and ease of implementation.

Author Contributions: Y.W., F.M., Z.Z., T.T. and E.P. carried out the calculations. Y.W., F.M., Z.Z., T.T., E.P., N.B. and C.W. wrote the paper. C.W. designed the research. All authors have read and agreed to the published version of the manuscript.

Funding: Y.W. is supported by the China Scholarship Council. C.W., N.B. and E.P. are supported by Grant EP/R02992X/1 from the U.K. Engineering and Physical Sciences Research Council (EPSRC).

Data Availability Statement: The codes are available at url dmft.ai (accessed on 12 December 2021) under the GPL 3.0 license.

Acknowledgments: This work was performed using resources provided by the ARCHER U.K. National Supercomputing Service and the Cambridge Service for Data Driven Discovery (CSD3) operated by the University of Cambridge Research Computing Service (www.csd3.cam.ac.uk), provided by Dell EMC and Intel using Tier-2 funding from the Engineering and Physical Sciences Research Council (Capital Grant EP/P020259/1), and DiRAC funding from the Science and Technology Facilities Council (www.dirac.ac.uk).

Conflicts of Interest: The authors declare no conflict of interest.

Appendix A

Table A1. Calculated structural parameters of the La–H and Ce–H compounds.

	Space Group	Lattice Parameters (Å)	Atoms	Atomic Coordinates (Fractional)		
				x	y	z
LaH16 (250 GPa)	P6/mmm	a = b = 3.52147	H(4h)	0.3333	0.6667	0.1811
		c = 3.55630	H(6i)	0.5000	0.0000	0.2522
		$\alpha = \beta = 90°$	H(6k)	0.7086	0.0000	0.5000
		$\gamma = 120°$	La(1a)	0.0000	0.0000	0.0000
CeH16 (250 GPa)	P6/mmm	a = b = 3.47980	H(4h)	0.3333	0.6667	0.1754
		c = 3.43362	H(6i)	0.5000	0.0000	0.2511
		$\alpha = \beta = 90°$	H(6k)	0.2890	0.0000	0.5000
		$\gamma = 120°$	La(1a)	0.0000	0.0000	0.0000

References

1. McMillan, P.F. Condensed matter chemistry under 'extreme' high pressure–High temperature conditions. *High Press. Res.* **2004**, *24*, 67–86. [CrossRef]
2. Miao, M.; Sun, Y.; Zurek, E.; Lin, H. Chemistry under high pressure. *Nat. Rev. Chem.* **2020**, *4*, 508–527. [CrossRef]
3. Wang, H.; Li, X.; Gao, G.; Li, Y.; Ma, Y. Hydrogen-rich superconductors at high pressures. *Wiley Interdiscip. Rev. Comput. Mol. Sci.* **2018**, *8*, e1330. [CrossRef]
4. Ashcroft, N. Hydrogen dominant metallic alloys: High temperature superconductors? *Phys. Rev. Lett.* **2004**, *92*, 187002. [CrossRef]
5. Ashcroft, N.W. Metallic hydrogen: A high-temperature superconductor? *Phys. Rev. Lett.* **1968**, *21*, 1748. [CrossRef]
6. Nakao, H.; Einaga, M.; Sakata, M.; Kitagaki, M.; Shimizu, K.; Kawaguchi, S.; Hirao, N.; Ohishi, Y. Superconductivity of pure H3S synthesized from elemental sulphur and hydrogen. *J. Phys. Soc. Jpn.* **2019**, *88*, 123701. [CrossRef]
7. Harshman, D.R.; Fiory, A.T. Compressed H3S: Inter-sublattice Coulomb coupling in a high-T c superconductor. *J. Phys. Condens. Matter* **2017**, *29*, 445702. [CrossRef]
8. Sun, D.; Minkov, V.S.; Mozaffari, S.; Sun, Y.; Ma, Y.; Chariton, S.; Prakapenka, V.B.; Eremets, M.I.; Balicas, L.; Balakirev, F.F. High-temperature superconductivity on the verge of a structural instability in lanthanum superhydride. *Nat. Commun.* **2021**, *12*, 1–7. [CrossRef]
9. Kostrzewa, M.; Szczęśniak, K.; Durajski, A.; Szczęśniak, R. From lah 10 to room–temperature superconductors. *Sci. Rep.* **2020**, *10*, 1–8. [CrossRef]
10. Yi, S.; Wang, C.; Jeon, H.; Cho, J.H. Stability and bonding nature of clathrate H cages in a near-room-temperature superconductor LaH 10. *Phys. Rev. Mater.* **2021**, *5*, 024801. [CrossRef]
11. Li, Y.; Hao, J.; Liu, H.; Li, Y.; Ma, Y. The metallization and superconductivity of dense hydrogen sulfide. *J. Chem. Phys.* **2014**, *140*, 174712. [CrossRef]
12. Drozdov, A.; Eremets, M.; Troyan, I.; Ksenofontov, V.; Shylin, S.I. Conventional superconductivity at 203 kelvin at high pressures in the sulphur hydride system. *Nature* **2015**, *525*, 73–76. [CrossRef]
13. Drozdov, A.; Kong, P.; Minkov, V.; Besedin, S.; Kuzovnikov, M.; Mozaffari, S.; Balicas, L.; Balakirev, F.; Graf, D.; Prakapenka, V.; et al. Superconductivity at 250 K in lanthanum hydride under high pressures. *Nature* **2019**, *569*, 528–531. [CrossRef]
14. Kong, P.; Minkov, V.S.; Kuzovnikov, M.A.; Drozdov, A.P.; Besedin, S.P.; Mozaffari, S.; Balicas, L.; Balakirev, F.F.; Prakapenka, V.B.; Chariton, S.; et al. Superconductivity up to 243 K in the yttrium-hydrogen system under high pressure. *Nat. Commun.* **2021**, *12*, 1–9. [CrossRef]
15. Sun, W.; Kuang, X.; Keen, H.D.; Lu, C.; Hermann, A. Second group of high-pressure high-temperature lanthanide polyhydride superconductors. *Phys. Rev. B* **2020**, *102*, 144524. [CrossRef]
16. Liu, L.; Wang, C.; Yi, S.; Kim, K.W.; Kim, J.; Cho, J.H. Microscopic mechanism of room-temperature superconductivity in compressed LaH 10. *Phys. Rev. B* **2019**, *99*, 140501. [CrossRef]
17. Heil, C.; Di Cataldo, S.; Bachelet, G.B.; Boeri, L. Superconductivity in sodalite-like yttrium hydride clathrates. *Phys. Rev. B* **2019**, *99*, 220502. [CrossRef]
18. Song, H.; Zhang, Z.; Cui, T.; Pickard, C.J.; Kresin, V.Z.; Duan, D. High Tc Superconductivity in Heavy Rare Earth Hydrides. *Chin. Phys. Lett.* **2021**, *38*, 107401. [CrossRef]
19. Sarma, S.D.; Li, Q. Many-body effects and possible superconductivity in the two-dimensional metallic surface states of three-dimensional topological insulators. *Phys. Rev. B* **2013**, *88*, 081404. [CrossRef]
20. Olalde-Velasco, P.; Jiménez-Mier, J.; Denlinger, J.; Hussain, Z.; Yang, W. Direct probe of Mott-Hubbard to charge-transfer insulator transition and electronic structure evolution in transition-metal systems. *Phys. Rev. B* **2011**, *83*, 241102. [CrossRef]
21. Plekhanov, E.; Zhao, Z.; Macheda, F.; Wei, Y.; Bonini, N.; Weber, C. Computational Materials Discovery for Lanthanide Hydrides at high pressure: Predicting High Temperature superconductivity. *arXiv* **2021**, arXiv:2107.12316.
22. Plekhanov, E.; Bonini, N.; Weber, C. Calculating dynamical mean-field theory forces in *ab initio* ultrasoft pseudopotential formalism. *Phys. Rev. B* **2021**, *104*, 235131. [CrossRef]
23. Wang, Y.; Lv, J.; Zhu, L.; Ma, Y. CALYPSO: A method for crystal structure prediction. *Comput. Phys. Commun.* **2012**, *183*, 2063–2070. [CrossRef]
24. Giannozzi, P.; Baroni, S.; Bonini, N.; Calandra, M.; Car, R.; Cavazzoni, C.; Ceresoli, D.; Chiarotti, G.L.; Cococcioni, M.; Dabo, I.; et al. QUANTUM ESPRESSO: A modular and open-source software project for quantum simulations of materials. *J. Phys. Condens. Matter* **2009**, *21*, 395502. [CrossRef]
25. Clark, S.J.; Segall, M.D.; Pickard, C.J.; Hasnip, P.J.; Probert, M.I.; Refson, K.; Payne, M.C. First principles methods using CASTEP. *Z. Krist.-Cryst. Mater.* **2005**, *220*, 567–570. [CrossRef]
26. Plekhanov, E.; Hasnip, P.; Sacksteder, V.; Probert, M.; Clark, S.J.; Refson, K.; Weber, C. Many-body renormalization of forces in f-electron materials. *Phys. Rev. B* **2018**, *98*, 075129. [CrossRef]
27. Lee, H.; Plekhanov, E.; Blackbourn, D.; Acharya, S.; Weber, C. The Mott to Kondo transition in diluted Kondo superlattices. *Commun. Phys.* **2019**, *2*, 1–8. [CrossRef]
28. Perdew, J.P.; Burke, K.; Wang, Y. Generalized gradient approximation for the exchange-correlation hole of a many-electron system. *Phys. Rev. B* **1996**, *54*, 16533. [CrossRef]

29. Perdew, J.P.; Chevary, J.A.; Vosko, S.H.; Jackson, K.A.; Pederson, M.R.; Singh, D.J.; Fiolhais, C. Atoms, molecules, solids, and surfaces: Applications of the generalized gradient approximation for exchange and correlation. *Phys. Rev. B* **1992**, *46*, 6671. [CrossRef]
30. Rappe, A.M.; Rabe, K.M.; Kaxiras, E.; Joannopoulos, J. Erratum: Optimized pseudopotentials [phys. rev. b 41, 1227 (1990)]. *Phys. Rev. B* **1991**, *44*, 13175. [CrossRef]
31. Baroni, S.; De Gironcoli, S.; Dal Corso, A.; Giannozzi, P. Phonons and related crystal properties from density-functional perturbation theory. *Rev. Mod. Phys.* **2001**, *73*, 515. [CrossRef]
32. Dynes, R. McMillan's equation and the Tc of superconductors. *Solid State Commun.* **1972**, *10*, 615–618. [CrossRef]
33. Allen, P.B.; Dynes, R. Transition temperature of strong-coupled superconductors reanalyzed. *Phys. Rev. B* **1975**, *12*, 905. [CrossRef]
34. Weber, C. Unifying guiding principles for designing optimized superconductors. *Proc. Natl. Acad. Sci. USA* **2021**, *118*, e2115874118. [CrossRef]
35. Parcollet, O.; Ferrero, M.; Ayral, T.; Hafermann, H.; Krivenko, I.; Messio, L.; Seth, P. TRIQS: A toolbox for research on interacting quantum systems. *Comput. Phys. Commun.* **2015**, *196*, 398–415. [CrossRef]
36. Aichhorn, M.; Pourovskii, L.; Seth, P.; Vildosola, V.; Zingl, M.; Peil, O.E.; Deng, X.; Mravlje, J.; Kraberger, G.J.; Martins, C.; et al. TRIQS/DFTTools: A TRIQS application for ab initio calculations of correlated materials. *Comput. Phys. Commun.* **2016**, *204*, 200–208. [CrossRef]